Theory of soft-x-ray-absorption thresholds: Amorphous Mg_xSb_{1-x} alloys and metallic Li, Na, Mg, and Al

John D. Dow*
Department of Physics and Materials Research Laboratory, University of Illinois at Urbana-Champaign, Urbana, Illinois 61801

John E. Robinson†
Argonne National Laboratory, Argonne, Illinois 60439

John H. Slowik‡‖
Department of Physics and Materials Research Laboratory, University of Illinois at Urbana-Champaign, Urbana, Illinois 61801
Xerox Corporation, Webster Research Center, Webster, New York 14580§

Bernd F. Sonntag‡ **
Department of Physics and Materials Research Laboratory, University of Illinois at Urbana-Champaign, Urbana, Illinois 61801
II. Institut für Experimentalphysik, Universität Hamburg, Hamburg, Germany§

(Received 28 January 1974)

The trends as a function of free-electron density, $n = [(4/3)\pi r_s^3 a^3]^{-1}$, in the soft-x-ray absorption spectra $\epsilon_2(\omega)$ of amorphous Mg_xSb_{1-x} alloys and metallic Li, Na, Mg, and Al are analyzed in terms of the many-electron theory of x-ray threshold anomalies: $\epsilon_2(\omega) = A\,\theta[(\hbar\omega - E_T)/\xi]^{-\alpha_l}$. The threshold exponents α_l are calculated as functions of r_s using the Nozières-deDominicis theory and a (Hulthén) screened-potential approximation to the electron-hole interaction. These calculated exponents are in marked disagreement with the empirical rule $\alpha_0 \simeq 0.068 r_s$ for Na, Mg, and Al. The cutoff energy ξ is extracted from Mg_xSb_{1-x} alloy data and, within experimental error, is independent of x. Thus ξ cannot be identified with a Fermi energy. The value $\xi = 0.24 \pm 0.1$ eV is too small to be identified as a conduction-band width, but could be identified with the exciton rydberg $R = 13.6(m/m_0\epsilon_0^2)$ eV, where m is the conduction-band mass and ϵ_0 is the static dielectric constant of Mg_3Sb_2. The analyses indicate the qualitative importance of final-state interactions in shaping the absorption thresholds, but improved, quantitatively accurate, theoretical understanding of the threshold exponents α_l and the characteristic energy ξ is needed. Future experiments on x-ray edges of alloys such as Mg_xSb_{1-x} should be coupled with independent experimental determination of the variation of r_s with composition x, in order to facilitate comparison of the many-electron theory with data.

I. INTRODUCTION

In one of the hallmark papers of contemporary many-electron theory,[1] G. D. Mahan proposed that electron-hole interactions force the soft-x-ray absorption and emission spectra of simple metals to exhibit shapes which either diverge or vanish at threshold. The identification in soft-x-ray spectra of peaks and shoulders, which appeared inexplicable in terms of calculated one-electron densities of states,[2] stimulated experimental interest in Mahan's theory at the same time that theorists recognized analogies between the x-ray theory and the Kondo effect.[3]

The over-all importance of Mahan's work to the modern many-body theory of solids, combined with its relevance to the understanding of x-ray spectra, provides ample motivation for subjecting it to the ultimate test of a physical theory: Can it quantitatively describe the data?

In this paper, we deduce some experimentally verifiable consequences of the present form of that theory and compare the theory with soft-x-ray absorption data for Na, Mg, Al, Li,[4] and amorphous alloys of Mg_xSb_{1-x}.[5,6]

The units of energy and length used in this paper are the exciton[7] rydberg R and Bohr radius a, respectively:

$$R = me^4/2\epsilon_0^2\hbar^2 = 13.6(m/m_0\epsilon_0^2)\ \text{eV}, \tag{1}$$

$$a = \hbar^2\epsilon_0/me^2 = 0.53(\epsilon_0 m_0/m)\ \text{Å}. \tag{2}$$

Here m and m_0 are the conduction-band effective mass and the free-electron mass, respectively; $e = -|e|$ is the electron charge, and ϵ_0 is the static dielectric constant of all bound electrons except the conduction-band electrons (e.g., in doped InSb, ϵ_0 would be the static dielectric constant of the pure material; in Na, ϵ_0 would be the computed[8] dielectric constant of the $1s^2 2s^2 2p^6$ cores).

The density n of the conduction-band electron gas is characterized by the reduced interelectron radius r_s:

$$\tfrac{4}{3}\pi(r_s a)^3 = n^{-1}. \tag{3}$$

Section II of this paper is devoted to a preliminary discussion of the Mahan theory, its relationship to the data of interest, and its relationship to the present paper. Section III contains a discussion of the parameters of the Mahan theory, principally the exponents α_l and the characteristic en-

ergy ξ. This section presents screened-potential model calculations of the Mahan exponents similar in spirit to work by Mahan,[9] Ausman and Glick,[10] and Longe[10]; the principal difference is that the calculations presented for metallic densities are self-consistent and are meant to be compared with *trends* in the data from material to material (Mahan, Ausman, and Glick were primarily interested in computing α_1 for lithium). Section IV is devoted to a comparison of the theory with the data. The principal conclusions of this paper are presented in Sec. V. Considerable relevant but peripheral material is included in the Appendixes: Theoretical results for $r_s \geq 5$ and < 5 are presented in Appendixes *A* and *B*, respectively. The spectra analyzed here and the procedures for fitting them are given in Appendixes C (for Li, Na, Mg, and Al) and D (for Mg_xSb_{1-x}).

II. PRELIMINARY DISCUSSION

One-electron theory, which neglects the final-state interactions of the electrons with the core hole, predicts an optical absorption $\epsilon_2(\omega)$ proportional to (i) a transition-matrix element squared, (ii) the density of final states, and (iii) a Fermi factor that forbids transitions to occupied states below the Fermi surface (see Fig. 1). For the experiments of interest, the one-electron matrix elements and densities of states are generally nonzero at threshold and contribute only an uninteresting constant factor, A^2, to the threshold law. Furthermore, in metals[11] Fermi energies generally exceed thermal energies by orders of magnitude, guaranteeing the adequacy of a zero-temperature theory and allowing the Fermi factor to be approximated by a step function. Thus, the one-electron theory yields a step-like threshold law:

$$\epsilon_2(\omega) = A^2\theta(\hbar\omega - E_T) \text{ for } \hbar\omega \approx E_T. \tag{4}$$

Mahan proposed that electron-hole final-state interactions modify the one-electron result, producing the singular threshold behavior[1,12]

$$\epsilon_2(\omega) = \sum_{l=0}^{\infty} A_l^2 \left(\frac{\hbar\omega - E_T}{\xi}\right)^{-\alpha_l} \theta(\hbar\omega - E_T). \tag{5}$$

Here $\epsilon_2(\omega)$ is proportional to the photoabsorption coefficient[13] for a photon of energy $\hbar\omega$, E_T is the threshold energy, ξ is a parameter with the dimensions of energy, and A_l^2 is proportional to the density of states multiplied by the squared-dipole transition matrix element from a core state to a conduction-electron state with angular momentum quantum number l. $\theta(x)$ is the unit step function and $2\pi\hbar$ is Planck's constant. Note that $\epsilon_2(\omega)$ diverges or vanishes at threshold depending on whether the dominant exponent α_l is positive or negative.

The many-electron result reduces to the one-electron approximation formula [Eq. (4)] in the limit of zero electron-hole interaction:

$$\alpha_l(\text{one-electron}) \equiv 0 \tag{6}$$

and

$$E_T(\text{one-electron}) = E_{gap} + E_F. \tag{7}$$

Here E_{gap} is the energy of the bottom of the conduction band relative to the center of the core band, and E_F is the Fermi energy relative to the bottom of the conduction band.

Mahan's threshold law, Eq. (5), with the many free parameters A_l, E_T, ξ, and α_l, is sufficiently flexible to fit almost any spectrum. In order to subject the theory to valid and rigid experimental tests, it is necessary to know the dependence of those parameters, especially the energy ξ and the exponents α_l, on experimental variables such as r_s, ϵ_0, and m. Of these, the most easily manipulated variable is r_s, since nature provides metals of different electron density (mostly, $2 < r_s < 5$) and controlled-composition alloys can be made with low densities, $r_s > 5$.

In Mahan's model, the electron density determines both the Fermi energy $E_F = \hbar^2 k_F^2/2m$ and the electron-hole interaction V_{eh}, which, for example, in the Thomas-Fermi approximation involves a screening wave vector proportional to $r_s^{-1/2}$. Once the variations of k_F and V_{eh} with r_s are known, the density dependence of the partial-wave phase shifts can be calculated and inserted into the Nozières-DeDominicis expression for the Mahan exponents[12]:

$$\alpha_l = 2\delta_l(k_F)/\pi - \Delta. \tag{8a}$$

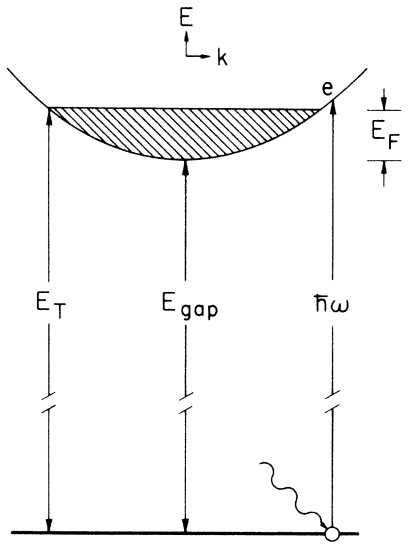

FIG. 1. Illustrating the x-ray transition discussed in this paper on an energy-band diagram E vs k. The photon creates a hole in a core level and an electron above the filled Fermi sea.

Here the "orthogonality catastrophe" is responsible for the term

$$\Delta = 2\sum_{j=0}^{\infty}(2j+1)[\delta_j(k_F)/\pi]^2 \qquad (8b)$$

and $\delta_l(k_F)$ is the phase shift experienced by a Fermi-energy electron scattered by V_{eh}; the central potential of the hole presumed fixed at the origin of coordinates. Such calculations are presented in Sec. III.

Recall that the primary (qualitative) successes of the Mahan theory have been based on the Nozières-DeDominicis formula: the apparent[14-17] explanation or prediction of (i) anomalous threshold "spikes" whenever the dominant α_l is positive, and (ii) rounded thresholds whenever the dominant α_l is negative. For a simple free-electron metal, the attractive electron-hole interaction generally causes the s-wave phase shift to be large and positive, giving a positive s-wave Mahan exponent: $\alpha_0 > 0$; the p-wave phase shift is usually much smaller than δ_0, and the "orthogonality catastrophe"[12,18] contribution to the exponent $-\Delta$ is thought to force the p-wave exponent to be negative: $\alpha_1 < 0$. (Similar considerations yield $\alpha_l < 0$ for $l \geq 2$.) Thus, for allowed transitions to s-like conduction-band states, A_0 is nonzero, α_0 is positive, and a divergent spike-like threshold anomaly is expected. For those metals in which transitions to s-states are forbidden (e.g., $A_0 \equiv 0$, that is, s-like and d-like holes), transitions to p states are allowed ($A_1 \neq 1$) and the p exponent (being larger than the exponents for larger l) dominates the threshold shape, causing it to be rounded whenever α_1 is negative.

In this paper, we consider x-ray absorption by metals and both x-ray and optical absorption by degenerate semiconductors. We are concerned with how such absorption depends on electron density.

The ideal system for testing the many-electron theory would be a semiconductor, such as InSb, but with valence-band mass m_h sufficiently heavy to satisfy Mahan's recoilless-hole criterion $m \ll m_h$. By varying the concentration of n-type dopants, the degeneracy of the conduction-band Fermi sea could be controlled over the range $0.1 \lesssim r_s < \infty$. The optical transitions in such doped semiconductors would correspond to the Mahan theory, which assumes only the effective-mass approximation, a localized hole, and a free degenerate gas of electrons. With increasing Fermi energy a Burstein edge effect[19] should be observed, with the Mahan anomaly shaping the absorption threshold. To date, many-electron threshold anomalies have been detected only in soft-x-ray spectra; none have been observed in the optical spectra of degenerate semiconductors.

The principal observations of anomalies thought to be caused by the Mahan effect have occurred in light metals: Na, Mg, Al, and Li.[4] In applying the many-electron theory to these materials, we follow other authors[9,10] and assume the metals to be theoretically identical to heavily doped semiconductors, but with background dielectric constants ϵ_0 nearly unity, as computed from the polarizability of the closed-shell cores. Within the context of the many-electron theory, the primary difference between a metal and a semiconductor is the difference in background dielectric constants: $\epsilon_0 = \approx 15$ for a semiconductor and $\epsilon_0 \approx 1$ for metal. The larger dielectric constants and normally smaller conduction-band masses generally cause the semiconductors to exhibit large exciton radii, $a = \hbar^2\epsilon_0/me^2$, putting them into the Wannier-Mott-Elliott effective-mass weak-binding limit. Although the exciton radii of metals, computed from the expression $a = \hbar^2\epsilon_0/me^2$, more nearly approximate the Frenkel limit ($a \approx$ lattice constant), we follow previous authors and treat the final-state interactions in metals within the effective-mass model.[1]

In this paper, we also treat the x-ray threshold anomalies of Mg_xSb_{1-x} amorphous alloys. Since most of the relevant data for these materials correspond to values of x near the intermetallic compound composition ($x = 0.6$), we assume the "host" to be Mg_3Sb_2, with "impurities" of Mg and Sb supplying the population of the presumed-free-electron-like conduction band. Thus the dielectric constant ϵ_0 and effective mass m used in calculating the exciton radius and binding energy are the values for crystalline Mg_3Sb_2. Since the core hole is massive, m is the electron's band effective mass, $m \approx 3.1m_0$.[20] Unfortunately ϵ_0 is not known; but realizing that crystalline Mg_3Sb_2 is a semiconductor (its band gap is 0.82 eV),[21] it would be reasonable to guess $\epsilon_0 \approx 13$.[22] Therefore we obtain $R \approx 0.25$ eV.[23,24]

The data cited as evidence for Mahan's threshold effect are enhanced $L_{2,3}$ absorption edges ($\alpha_0 > 0$) of Mg_xSb_{1-x} and Mg_xBi_{1-x} alloys,[5,6] $L_{2,3}$ edges of Na, Mg, and Al,[4] and K edges ($\alpha_1 < 0$) of Li,[4] Al,[25-27] and (recently) Mg.[26]

Recent experimental and theoretical developments, however, cause us to reexamine the many-electron interpretation of the soft-x-ray threshold anomalies.

On the experimental side: (i) soft-x-ray absorption measurements of amorphous alloys have yielded spectra whose dependences on electron density can be tested against the theory; (ii) soft-x-ray absorption measurements by Wolff *et al.*[28] on Na *vapor* have revealed a sharp line at precisely the energy of the anomalous spike in the solid's spectrum, making one wonder if the solid's spike is a many-electron or few-electron phenomenon. Of course, the absorption lines for both the atom and the solid have common parentage and *should* reside

at approximately the same energy; but the possibility that the solid's spike is, in fact, a simple localized quasiatomic absorption should not be overlooked—a possibility that might be more at odds with the formulation of the Mahan theory in momentum space than with the theory itself; and (iii) an attempt to convert the rounded Li absorption edge into a spike by destroying inversion symmetry has failed,[29] although the many-electron theory had predicted that it should not have.[30]

On the theoretical side: (i) The many-electron interpretation of the Li anomaly has been criticized, and alternate explanations have been proposed—attributing the anomaly to either a gigantic electron-amplified simulated phonon broadening of the core-state or an Auger effect.[31] Both phonon and Auger effects give an absorption edge shape in quantitative agreement with the data—whereas the many-electron theory fails to achieve even good qualitative agreement,[31] producing nonoverlapping absorption and emission spectra with incorrect slopes at threshold. (ii) Arguments based only on the Friedel sum rule and the relative impenetrability of the hole's angular momentum barrier to d-wave electrons reveal that the rounded hard-x-ray K spectra and the spiked soft-x-ray $L_{2,3}$ edges of aluminum and magnesium have shapes that cannot both be consistent with the Nozières-DeDominicis expression for the exponents α_l [Eq. (8)] and the interpretation $\alpha_0 > 0$, and $\alpha_1 < 0$.[32,33] Thus the belief that aluminum and magnesium support the many-electron theory by exhibiting both enhanced $L_{2,3}$ edges and orthogonality-catastrophe suppressed K edges is no longer tenable. (iii) Compatibility relationships[32] between K and L edges, based on the Nozières-DeDominicis expression [Eq. (8)] indicate that K edges can be suppressed ($\alpha_1 < 0$) only if the s-wave phase shift at the Fermi surface is near resonance [$\delta_0(k_F) \approx \frac{1}{2}\pi$], a fact that suggests the existence of a bound exciton state[34] [$\delta_0(0) = \pi$] and implies an s-wave ($L_{2,3}$-edge) exponent $\alpha_0 \approx \frac{1}{2}$. The emission spectra of simple metals offer no evidence of such bound exciton states, and $L_{2,3}$-edge exponents are generally considerably smaller than one-half. Thus the principal experimentally relevant conclusion of the many-electron theory, that $L_{2,3}$ edges are generally enhanced whereas K edges are suppressed, lacks a rigorous theoretical foundation,[16,33]

Clearly, *quantitative* comparisons of the Mahan theory with the data are needed in order to determine which spectra exhibit genuine many-electron anomalies. With the dual interpretation of K-edge rounding and L enhancement under attack, it is desirable to concentrate on the soft-x-ray $L_{2,3}$ edges and to determine the extent to which they distort with changes of free-electron density. It is the purpose of this paper to attempt such quantitative comparison as is presently possible and to discuss the dependences on r_s of the soft-x-ray anomalies of metallic Na, Mg, Al, and Li, and of Mg_xSb_{1-x} alloys.

III. PARAMETERS OF MAHAN THEORY

Of the parameters A_l, E_T, ξ, and α_l of the Mahan theory [see Eq. (5)] A_l and E_T are finite in the limit $e^2/\epsilon_0 \to 0$ and are sufficiently insensitive to the final-state interactions to render impractical the detection of differences between their one-electron and many-electron values—especially in view of the present primitive state of one-electron theory. Therefore only the critical exponents α_l and the characteristic energy ξ are amenable to close scrutiny and we shall concentrate on determining their dependences on effective mass, dielectric constant, and Fermi energy.

A. Exponents α_l

The critical exponent of the Mahan theory is given by[12]

$$\alpha_l = \frac{2\delta_l(k_F)}{\pi} - 2\sum_{j=0}^{\infty}(2j+1)\left(\frac{\delta_j(k_F)}{\pi}\right)^2. \tag{9}$$

The $\delta_l(k_F)$ are the partial-wave phase shifts at the Fermi surface ($E_F = \hbar^2 k_F^2/2m$) obtained from the scattering solutions of the single-electron Schrödinger equation

$$[(-\hbar^2/2m)\nabla^2 + V_{eh}]\psi_{\vec{k},l}(\vec{r}) = E_{\vec{k}}\psi_{\vec{k},l}(\vec{r}). \tag{10}$$

Here V_{eh} is the effective electron-hole interaction and should include Friedel oscillations, the nonlocal and dynamical effects of pair excitations, and a short-ranged repulsive pseudopotential which maintains the orthogonality of the conduction-band states to the core. In the interest of simplicity, Mahan and others[9,10] took V_{eh} to be a Yukawa-like statically screened local potential:

$$V_{eh}(r) \approx -(Ze^2/\epsilon_0 r)\, e^{-k_s r}. \tag{11}$$

Here $Z = 1$ is the charge of the hole and k_s is the screening wave vector; if we were to determine k_s using Fermi-Thomas self-consistent-field theory (which we shall *not* do), it would have the value[35]

$$k_s^{FT} a = \left(\frac{6\pi n a^2 Z e^2}{\epsilon_0 E_F}\right)^{1/2} = \left(\frac{12}{\pi}\right)^{1/3}\left(\frac{Z}{r_s}\right)^{1/2} = 1.563\left(\frac{Z}{r_s}\right)^{1/2}. \tag{12}$$

Here E_F and k_F are the Fermi energy and wave vector, respectively:

$$E_F = \frac{\hbar^2 k_F^2}{2m} = \left(\frac{9\pi}{4}\right)^{2/3} r_s^{-2} R = 3.683 r_s^{-2} R, \tag{13}$$

$$k_F a = (\tfrac{9}{4}\pi)^{1/3} r_s^{-1} = 1.919 r_s^{-1}. \tag{14}$$

To gain the analytic simplicity of an exactly-

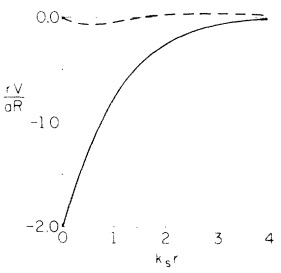

FIG. 2. Solid line: $rV(r)$ vs $k_s r$ for the Hulthén potential $V = V_{eh}$ of Eq. (15) with $Z = 1$; dashed line: $rV(r)$ vs $k_s r$ for V the difference between Hulthén and Fermi-Thomas potentials [Eqs. (15) and (11)] with $Z = 1$. Units: rydberg R and Bohr radius a [Eqs. (1) and (2)].

soluble s-wave problem, we replace the Yukawa form of the screened potential used by Mahan and others with a potential of the Hulthén form[36]:

$$V_{eh}(r) = \frac{-Ze^2 k_s \pi^2/6\epsilon_0}{\exp(\frac{1}{6}k_s\pi^2 r) - 1} = \frac{-\frac{1}{3}Zk_s a\pi^2 R}{\exp(\frac{1}{6}k_s\pi^2 r) - 1}. \quad (15)$$

Note that the Hulthén potential is virtually indistinguishable from the Yukawa potential (Fig. 2) when, as in Eq. (15), the integral of $rV_{eh}(r)$ over all space is the same for both potentials. Further, at all distances, even down into the deep Coulomb well near a point charge, the random-phase-approximation potential just oscillates weakly about the Thomas-Fermi as a local average,[35] and the Hulthén shape is as adequate to our present purposes as the full linear response shape. To be sure, at sufficiently large r_s, it may be that none of these shapes can self-consistently accommodate the multiple scattering off the bare potential, but an adequate study of this possibility requires use of rather elaborate nonlinear response theory and has not yet been made.

The primary advantage of the Hulthén potential is that its s-wave phase shift can be evaluated exactly:

$$\delta_0(k) = \arg\frac{\Gamma(u+1)\Gamma(v+1)}{\Gamma(u+v+1)}. \quad (16)$$

Here we have

$$u = [-ika + (\tfrac{1}{3}Zk_s a\pi^2 - k^2a^2)^{1/2}]/\tfrac{1}{6}k_s a\pi^2 \quad (17)$$

and

$$v = [-ika - (\tfrac{1}{3}Zk_s a\pi^2 - k^2a^2)^{1/2}]/\tfrac{1}{6}k_s a\pi^2. \quad (18)$$

The branch of the argument function arg to be used is best specified by Levinson's theorem[37]:

$$\delta_0(0) = n'\pi, \quad (19)$$

where n' is the number of bound s states

$$n' = \text{int}[(2/\pi)(3Z/k_s a)^{1/2}] \quad (20)$$

and int here indicates the greatest integer function.

We assume that the phase shifts for p and higher-angular momentum waves are accurately evaluated in the Born approximation, an assumption justified both by Mahan's computations and by ours for electron gases considerably more degenerate than those which support bound p states ($r_s \lesssim 20$).

In adopting this screened-potential model, we are aware of its limitations. We rely upon the model only to accurately predict general *trends* in the x-ray edge data, but do not expect it to produce a precise value of any particular quantity, such as the exponents α_l for a specific metal.

In discussing the screened-potential model, we shall consider two distinct regimes of conduction-band Fermi-gas density: (i) the low-density regime[38] ($r_s \geq 5$); and (ii) the ultradense to metallic-density regime ($0 < r_s < 5$). The low-density screened-potential calculations will be performed in a linear-response approximation similar to the usual[9,10] Fermi-Thomas approximation and, as such, will not be fully self-consistent, since at these densities it is possible for a screened potential to bind an electron, locally depleting the conduction-band charge. The high-density computations will be fully self-consistent for the case of weak scattering of p and higher-angular momentum waves; the computed phase shifts will satisfy Friedel's sum rule. Details of our computations are presented in Appendixes A (for $r_s \geq 5$) and B (for $r_s < 5$).

1. *Screening wave vector k_s for $r_s \geq 5$: Linear-response approximation*

For large r_s (low-density electron gas), the screening wave vector k_s will be determined by the Friedel sum rule, with the phase shifts all evaluated in Born approximation

$$Z = \frac{2}{\pi}\sum_{l=0}^{\infty}(2l+1)\delta_l^{\text{Born}}(k_F), \quad (21)$$

$$\delta_l^{\text{Born}}(k) = -\frac{k}{Ra^2}\int_0^\infty V(r)\, j_l^2(kr) r^2 dr, \quad (22)$$

where $j_l(x)$ is the spherical Bessel function and V is the Hulthén potential [Eq. (22)]. We shall refer to such screening as *linear-response screening*. Thus we have[39] the linear-response screening wave vector

$$k_s^L a = \frac{12}{\pi^2}\left(\frac{2Z\zeta(3)k_F a}{\pi}\right)^{1/2}, \quad (23a)$$

$$k_s^L a = \frac{12}{\pi^2}\left(\frac{2Z\zeta(3)}{\pi}\right)^{1/2}\left(\frac{9\pi}{4}\right)^{1/6} r_s^{-1/2} = 1.473(Z/r_s)^{1/2}, \quad (23b)$$

where $\zeta(3) = 1.202$ is the Riemann ζ function. Note that k_s^L is insignificantly different from the Fermi-Thomas screening wave vector k_s^{FT} [Eq. (12)].

Linear-response screening is of limited validity; and the actual phase shifts at the Fermi energy

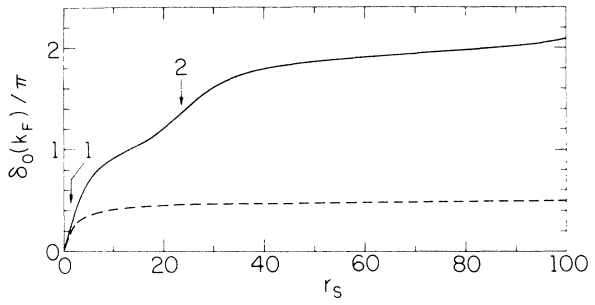

FIG. 3. Calculated Fermi-energy s-wave phase shift $\delta_0(k_F)$ vs r_s. Solid line: Hulthén value, Eq. (16); dashed line: Born approximation, Eq. (22); linear-response screening. The values of r_s at which the $2s$ and $1s$ exciton move into the continuum are marked 2 and 1, respectively.

may differ significantly from the Born-approximation values. Hence the low-density ($r_s > 5$) theory treated here is not fully self-consistent, but has a range of validity similar to that of the Fermi-Thomas theory. Note that the Fermi-energy s-wave phase shifts evaluated using Eq. (16) (Fig. 3) differ significantly from the Born-approximation values and that the Freidel sum rule is therefore unsatisfied.

2. *Screening wave vector k_s for $r_s < 5$: Self-consistent approximation*

For metallic densities ($2 < r_s < 5$) and ultradegenerate electron gases ($r_s \leq 2$) the screening wave vector k_s in the Hulthén potential [Eq. (15)] will be determined self-consistently using the Friedel sum rule

$$Z = \frac{2}{\pi}\sum_{l=0}^{\infty}(2l+1)\delta_l(k_F), \tag{24}$$

with the s-wave phase-shifts evaluated exactly [Eq. (16)] and higher angular momentum phase shifts evaluated in the Born approximation:

$$Z = [2/\pi][\delta_0(k_F) - \delta_0^{\mathrm{Born}}(k_F)] + Z[k_s^L/k_s]^2. \tag{25}$$

Owing to the implicit dependence of the phase shifts δ_0 and δ_0^{Born} on k_s, this is a transcendental equation for k_s which can be solved graphically or numerically.[40] Thus we fix r_s, compute k_F and k_s^L, and solve Eq. (25) for k_s. The resulting values of k_s are plotted in Fig. 4.

3. *Determination of Mahan exponents*

Once the screening wave vector k_s has been determined, it is straightforward to evaluate the Mahan exponents using the Nozières-DeDominicis expression [Eq. (8)]. Note that we hypothesize the applicability of Eq. (8) in the low-density regime, although the Nozières-DeDominicis evaluation presumes conduction electrons sufficiently mobile to fully screen the hole and phase shifts satisfying Friedel's sum rule.

B. Characteristic energy ξ

The role of the characteristic energy in the many-electron theory is both essential and curious; for, although it enters the formal theory as a mathematical cutoff, a theory with physical content cannot depend on an unphysical energy. Thus if the Mahan–Nozières-DeDominicis (MND) theory is to describe data, then ξ must be identified with some energy or combination of energies; these include the Fermi energy E_F, the exciton rydberg R, the conduction-band width W_c, and the inverse of the density of states at the Fermi energy (which for a parabolic conduction band is expressible in terms of the Fermi energy).

Different theories assign various values to ξ. For example, pseudopotential perturbation theoretic studies by Brouers, Longe, and Bergersen[41] indicate that ξ is a somewhat complicated function of E_F; and Friedel found $\xi = E_F$, using a somewhat different perturbation expansion.[42] However, perturbation theory necessarily diverges and is asymptotically valid only in the high-density limit ($r_s \to 0$), whereas real metals correspond to $2 \lesssim r_s \lesssim 5$. Pardee and Mahan[43] have recently identified ξ with the Fermi energy. However, the Pardee-Mahan identification represents an unconventional use of Watson's final-state-interaction theorem[44] and seems to imply that the MND theory is valid in the limit of infinitesimal Fermi energy, whereas the Elliott exciton theory[45] is known to be superior in that regime. The argument that ξ is a conduction-band width[46] also runs into difficulties in the exciton limit ($r_s \to \infty$). In that limit, the Elliott theory of optical absorption produces an absorp-

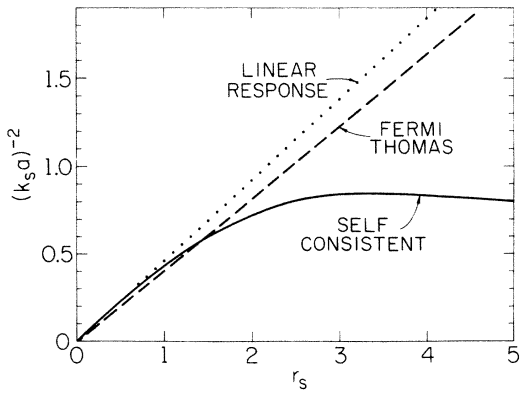

FIG. 4. Screening wave vector k_s, plotted as $(k_s a)^{-2}$ vs r_s. Solid, dashed, and dotted lines are self-consistent approximation, Fermi-Thomas approximation, and linear-response approximation, respectively.

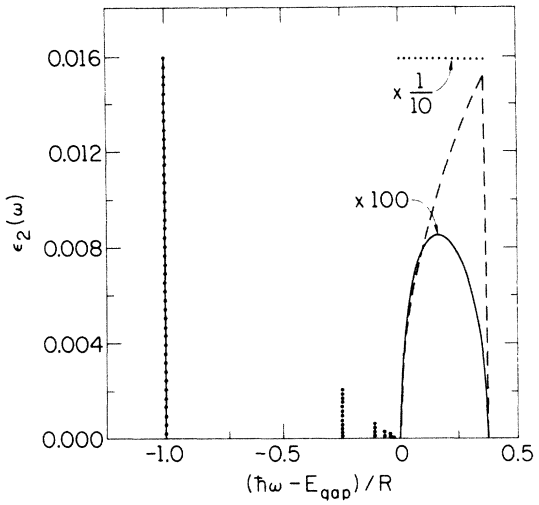

FIG. 5. Unbroadened exciton-limit theoretical optical absorption $\epsilon_2(\omega) = M\sum_\nu |\psi_\nu(0)|^2 \delta(\hbar\omega - E_{gap} - E_\nu)$ vs energy, $E = (\hbar\omega - E_{gap})/R$, normalized such that $M = 1$ in units with $R = 1 = a$. Dashed line: Assumed density of states, Eq. (13) with $\xi = 5$ eV; dotted line: exciton absorption (δ functions are normalized independent of the continuum to which they join continuously); solid line: contact-exciton approximation to exciton absorption: $\epsilon_2(E) = \mathrm{Im}(\epsilon^0(E)/[1 - \epsilon^0(E)/\epsilon^0(-1)])$, where $N_c(E) = \mathrm{Im}\epsilon^0(E)$. Note the enormous (factor of 1000) differences in the exciton and contact-exciton approximation line shapes for $E > 0$.

tion-band shape from the exciton Hamiltonian which differs by orders of magnitude from the shape produced from the MND Hamiltonians (see Fig. 5.).[47] The Hamiltonians differ only in that the MND theory approximates the Coulombic electron-hole interaction $-e^2/\epsilon_0 r$ by a δ function or separable potential. This approximation requires the introduction of an otherwise unnecessary energy cutoff, which is often identified with the conduction-band width. Thus, in the low-density limit ($r_s \to \infty$) with the effective-mass approximation, *the band-width cutoff is mathematical, not physical.* Finally, we note that in the low-density limit ($r_s \to \infty$, $E_F = 0$), even in its role as a mathematical cutoff, ξ is related to the strength of the electron-hole interaction.

TABLE I. Values for the critical exponent α_0 at various alloy compositions. The values are from Ref. 6 and have uncertainty ± 0.1. All samples were amorphous except for Mg, which was crystalline.

Composition	α_0
$Mg_{38}Sb_{62}$	0.30
$Mg_{43}Sb_{57}$	0.63
$Mg_{48}Sb_{52}$	0.55
$Mg_{58}Sb_{42}$	0.87
$Mg_{60}Sb_{40}$	1.04
$Mg_{67}Sb_{33}$	0.81
Mg	0.22

TABLE II. Exponents α_0 extracted from absorption-edge data of simple metals. [For Li, α_0 was determined by Eq. (34).]

Metal	r_s	α_0
Na	3.93	0.26 ± 0.04
Mg	2.65	0.18 ± 0.04
Al	2.07	0.15 ± 0.04
Li	3.25	0.48 ± 0.03

Thus it would be natural to replace the characteristic energy ξ by the exciton rydberg. However, in the high-density limit $r_s \to 0$ this is incompatible with perturbation theory.[41,42]

In summary, the present theoretical understanding of the cutoff ξ is incomplete; ξ is most likely a complicated function of R, E_F, and possibly W_c. Which dependence dominates the metallic and semiconducting regimes $2 \lesssim r_s$ will have to be determined experimentally.

IV. COMPARISON WITH DATA

We have argued that the Hulthén potential is an adequate model interaction so that we have [Eq. (16)]

$$\delta_0(k) = \arg \frac{\Gamma(u+1)\Gamma(v+1)}{\Gamma(1 - 12ik/k_s\pi^2)}, \tag{26}$$

where u and v are functions of k and k_s [Eqs. (17) and (18)], and the screening wave-vector is determined by the procedure of Sec. II. We insert this result into the Mahan form of the absorption threshold[48] [Eq. (5)]

$$\epsilon_2(\omega) = A^2 \left(\frac{\hbar\omega - E_T}{\xi}\right)^{-\alpha} \theta(\hbar\omega - E_T), \tag{27}$$

with the Nozières-DeDominicis exponent

$$\alpha_l = \frac{2\delta_l(k_F)}{\pi} - 2\sum_{j=0}^{\infty}(2j+1)\left(\frac{\delta_j(k_F)}{\pi^2}\right)^2 \tag{28}$$

to analyze the soft-x-ray absorption data. For the $L_{2,3}$ edges, α is α_0; for the K edges, $\alpha = \alpha_1$.[48]

The data of interest are (i) the $L_{2,3}$ absorption edges of Na, Mg, and Al, (ii) the K absorption edge of Li, and (iii) the $L_{2,3}$ absorption edges of amorphous alloys of Mg_xSb_{1-x}. These data are reproduced in Appendix D. Except for Li, we fit the data with the Mahan threshold shape (Gaussian broadened),[49] and thus determine[5] the values of the exponents α, which are tabulated in Tables I and II. The fitting procedures are discussed in Appendixes C and D. The exponent α_1 used to calculate α_0 for Li has been obtained by Yue and Doniach.[50]

Observe that the fact that the spectra can be analyzed in terms of the Mahan shape, by itself, does not necessarily indicate that final-state interactions

influence these spectra. The parameter $A^2\xi^\alpha$ governs the line strength, whereas α is essentially an inverse linewidth for asymmetric broadening. Several physical processes distinct from the Mahan mechanism could produce a line shape easily fit with the Mahan form, suitably broadened. To determine the extent to which the spectra are well-described by the Mahan theory, the dependences of α and ξ on electron density or r_s must be studied.

A. Exponents α_l

A highly sensitive test of the many-electron theory is provided by the exponents α_l.[51] The Nozières-DeDominicis result, Eqs. (5) and (8), which expresses the exponents as functions of the phase shifts, can be verified or excluded once the dependence of phase shifts of conduction electron density or r_s is known.

1. *Low densities*: $r_s > 5$

The L threshold exponents for Mg_xSb_{1-x} have been obtained by Slowik and Brown for various amorphous alloy compositions x and are listed in Table I. By taking published data[52] on resistivity as a function of composition x, it is possible to obtain the functional dependence of the exponent on resistivity, $\alpha(\rho)$, for Mg_xSb_{1-x}. To convert this dependence of exponent on resistivity to a dependence on r_s (or density), it would be necessary to know the variation of mobility μ with r_s:

$$\rho = (ne\mu)^{-1} = 4\pi(r_s a)^3/3e\mu(r_s). \tag{29}$$

Unfortunately, the mobility function $\mu(r_s)$ is presently unknown, so that only a qualitative comparison of the Mg_xSb_{1-x} exponents with the theory is possible. Normally one expects μ to be a decreasing function of r_s and hence ρ to be a monotonically increasing function of r_s.[53] Under ordinary circumstances,[54] the mobility may be expected to vary most rapidly with r_s if it is limited by charged defect scattering. For a simple band and with Thomas-Fermi screening, $\mu(r_s)$ decreases over the range $2.5 < r_s < 5$ by at most a factor of 4. Band-structure complications modest enough that the Nozières-DeDominicis derivation need not be modified could add only another factor of order unity.[55]

The Mg_xSb_{1-x} exponent data are plotted as a function of resistivity in Fig. 6. Note that the data separate into two distinct regions: (i) the low-density high-resistivity ($\rho > 10^2\ \Omega$ cm) large-r_s regime, where we have $\alpha_0 \approx -0.08 + 0.075\ \ln\rho$; and (ii) a metallic-density low-resistivity ($\rho < 10^{-4}\ \Omega$ cm) regime.[56] It is quite possible that, as a function of r_s, the distinct separation does not occur, but that the mobility as a function of composition decreases dramatically as electron motion ceases to be coherent, causing the resistivity to jump from 10^{-4} to $10^2\ \Omega$ cm. Hence it is not possible to state conclusively whether or not the Mg_xSb_{1-x} exponents α_0 are continuous functions of r_s.[56,57]

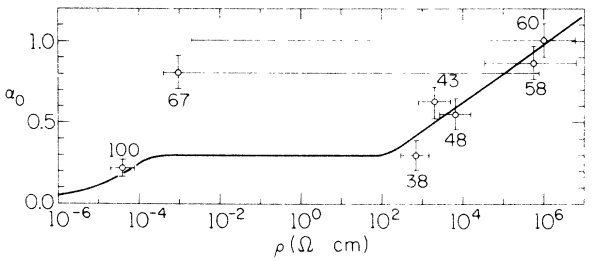

FIG. 6. Mg_xSb_{1-x} exponents α_0 vs resistivity ρ in ohm cm. The values of $y \equiv 100x$ are depicted on the graph. For $\rho < 10^{-4}\ \Omega$ cm, the curve corresponds to the empirical rule $\alpha_0 \approx 0.068 r_s$, assuming constant mobility. The data for $\rho > 100\ \Omega$ cm are approximately described by $\alpha_0 \approx 0.075 \ln\rho - 0.087$. The resistivity increases abruptly from 10^{-3} to $100\ \Omega$ cm for x between 0.67 and 0.60, hence the anomalously large error bars on the data for $y = 60$ and 67 (see Ref. 56). Furthermore the mobility might exhibit an edge between $y = 60$ and 67, in which case the datum for $y = 67$ might lie within the regime described by the empirical rule, Eq. (33).

The noteworthy feature of Fig. 6 is that the exponent α_0 appears to increase as the resistivity increases, in qualitative accord with the theoretical notion that final-state-interaction effects should increase with r_s. However, the theory indicates that α_0 should not be monotonic, but rather should exhibit a maximum[15] (less than $\alpha_0 = \frac{1}{2}$) for $\delta_0(k_F) \approx \frac{1}{2}\pi$:

$$\alpha_0 < 2[\delta_0(k_F)/\pi] - 2[\delta_0(k_F)/\pi]^2 \leq \tfrac{1}{2}. \tag{30}$$

Now several of the Mg_xSb_{1-x} exponents exceed $\frac{1}{2}$, and therefore cannot be computed from the Nozières-DeDominicis formula.

Furthermore, even in the unlikely case that the extracted exponents have been overestimated by a factor of 2 and that the Nozières-DeDominicis formula is applicable to amorphous Mg_xSb_{1-x} alloys, the fact that $\alpha_0(\rho)$ is experimentally a monotonic function of resistivity ρ indicates that $\alpha_0(\rho)$ as a function of ρ does not yet pass through its maximum value of $\frac{1}{2}$ even for the highest resistivity material ($Mg_{60}Sb_{40}$). In terms of $r_s(\rho)$, $r_s^{\max} \equiv r_s(10^6\ \Omega$ cm) is sufficiently small that $\alpha_0(r_s)$ is monotonically increasing for $r_s < r_s^{\max}$. Noting that theoretically $\delta_0(k_F)$ is a monotonically increasing function of r_s (Fig. 3), we have [using Eq. (30)]

$$\delta_0(k_F;\ r_s^{\max}) < \tfrac{1}{2}\pi \tag{31}$$

or (see Fig. 3)

$$r_s^{\max} \lesssim 5. \tag{32}$$

Thus, although the resistivity of the amorphous

Mg_xSb_{1-x} alloys varies over more than ten orders of magnitude, to describe the data with the existing theory, $r_s = 2.64$ (for Mg) to $r_s < 5$. Such a variation corresponds approximately to only one order of magnitude (a factor of 6.8) variation in charge density per ten orders variation of resistivity, an unacceptably small change of density. The net conclusion is that even in the unlikely case that the absolute magnitudes of the extracted Mg_xSb_{1-x} exponents might be in error by a factor of 2, the variation of those exponents with resistivity would be too small to conform to the Nozières-De-Dominicis theory of the Mahan exponent.

In anticipation of a result to be obtained from the Na, Mg, and Al data, we note that the empirical rule $\alpha_0 \approx 0.068 r_s$ can describe the Mg_xSb_{1-x} exponents if (i) the mobility as a function of x decreases abruptly by six orders of magnitude as the resistivity increases from 2×10^{-4} to 2×10^{2} Ω cm; and (ii) the mobility decreases slowly by a factor of ≈ 300 as the resistivity increases from 10^3 to 2×10^6 Ω cm.

We summarize the conclusions to be drawn from the exponents of amorphous Mg_xSb_{1-x}: (i) α_0 appears to be a single-valued function of resistivity—indicating the importance of conduction electron density and final-state interactions in shaping the x-ray threshold; (ii) the Nozières-DeDominicis expression for the exponents does not describe the data; and (iii) quantitative comparison of the Mg_xSb_{1-x} data will be possible only after $r_s(x)$, or the electron density or mobility as a function of amorphous-alloy composition is known.

Finally we note that at metallic compositions the electron density as a function of composition, and hence $r_s(x)$, can be determined from the Hall coefficient. At more insulating compositions, e.g., Sb-rich Mg_xSb_{1-x}, it may prove possible to determine $r_s(x)$ from direct measurement of drift mobility using the transient technique.[58] Thus $\alpha(r_s)$ could be directly determined for comparison with theory.

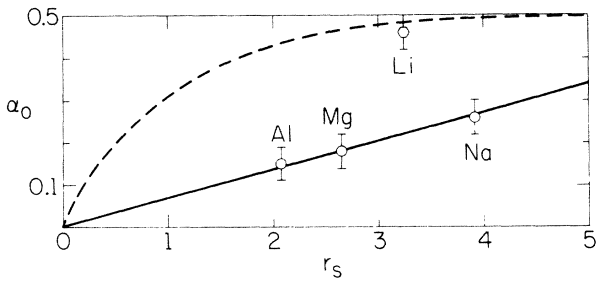

FIG. 7. Exponents α_0 vs r_s. Dashed line: theory, self-consistent approximation; solid line: empirical rule $\alpha_0 \approx 0.068 r_s$, determined by the data for Al, Mg, and Na (circles).

2. *High densities*: $r_s < 5$

In contrast to the case of amorphous alloys, such as Mg_xSb_{1-x}, the free-electron densities of simple metals are well known and it is possible to plot the extracted exponents α_0 as a function of r_s (Fig. 7). Observe the empirical rule,[59] which fits the Na, Mg, and Al data in Table II well (solid line),

$$\alpha_0(r_s) \approx 0.068 r_s. \tag{33}$$

The theory (dashed line) has an incorrect shape, incorrect slope near $r_s = 0$ and is generally too large, but reproduces the trend that α_0 increases as a function of r_s.

The exponent $\alpha_0 = 0.48$ plotted for Li has not been extracted directly from the data. Rather, the compatibility relationship[15]

$$\alpha_0 = \alpha_1 - \tfrac{1}{3} + \tfrac{2}{3}(1 - 6\alpha_1)^{1/2} \tag{34}$$

has been used to determine α_0 from the Doniach-Yue exponent[50] $\alpha_1 = -0.3$.

The fact that the exponents α_0 for Na, Mg, and Al are smooth functions of r_s suggests that conduction electron density and final-state interactions influence the shape of the x-ray threshold. However, this conclusion is tenable *only if the s-exponent for* Li, $\alpha_0 \approx 0.48$, *can be discarded*; that is, if the compatibility relationships are inapplicable to Li.

Observe that the empirical rule $\alpha_0 \approx 0.068 r_s$ is poorly described by the theory (Fig. 7); no obvious modifications of the form of the electron-hole interaction produce satisfactory agreement between the theory and the data. For example, in Born approximation, the empirical rule seems to imply an electron-hole interaction with a range proportional to r_s.[59] Of course, these conclusions are based on highly-simplified models of screening and must be regarded as tentative until calculations are available which account for Friedel oscillations, nonlinear response, band-structure, exchange, and correlation.

B. Characteristic energy ξ

The characteristic energy can be extracted from the spectra of Mg_xSb_{1-x} alloys. The exponents, independently determined,[5,6] are listed in Table I for various values of x. The spectra were fitted with the threshold law, Eq. (5). Defining

$$\hbar\Omega = E_T + 1 \text{ eV}, \tag{35}$$

we have

$$\ln\epsilon_2(\Omega) = \alpha_0 \ln\frac{\xi}{1 \text{ eV}} + 2\ln A. \tag{36}$$

In Fig. 8, we show a semilogarithmic plot of $\epsilon_2(\Omega)$[60] vs α_0 for various alloy concentrations x. Within experimental error, the data appear to lie along a straight line,[60] indicating that ξ is independent of composition x. The value of ξ estimated from the

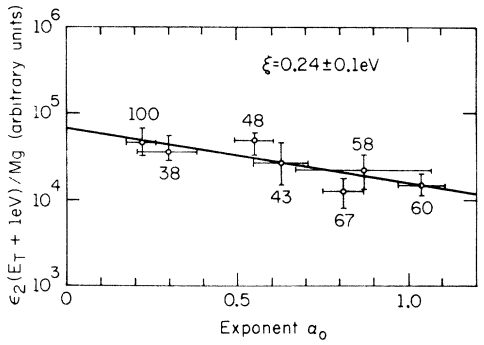

FIG. 8. Semilogarithmic plot of the fit to absorption per Mg atom, $\epsilon_2(\Omega)/\mathrm{Mg}$, (in arbitrary units) for $\hbar\Omega = E_T + 1$ eV vs α_0 for the Mg_xSb_{1-x} exponents of Table I (see Ref. 60). The straight line through the data corresponds to the optimum fit, $\xi = 0.24 \pm 0.1$ eV. Note that any smooth curve through the data would have negative slope everywhere, corresponding to $\xi < 1$ eV. The values $y \equiv 100x$ label each datum.

slope is

$$\xi = 0.24 \pm 0.1 \text{ eV}. \tag{37}$$

Furthermore, we find that A^2 corresponds to an absorption coefficient of 6.5×10^4 cm$^{-1} \pm 50\%$, a quite reasonable value. We emphasize that the slope of *any* smooth continuous curve through the data would be negative; that is, $\xi < 1$ eV.[61]

An extracted value of ξ less than 1 eV implies that the physical replacement of the mathematical cutoff is not a band width. Moreover, the apparent near constancy of the energy ξ deduced from the data also excludes ξ from being the Fermi energy, which should vary considerably with composition x. Thus the only natural energy which can be identified with ξ is the exciton Ryberg, which should be smaller than 1 eV because of the large dielectric constant ϵ_0 of the intermetallic compound Mg_3Sb_2.[62]

The flexibility of the Mahan threshold law, with free parameters A, ξ, α, and broadening Γ, precludes us from definitely stating that Fig. 6 demonstrates the applicability of Mahan's theory, although that figure certainly implies that the Mg_xSb_{1-x} x-ray data are not inconsistent with Mahan's threshold law and a constant cutoff, ξ.

The principal conclusion to be drawn from Fig. 8 is that *either the energy ξ is smaller than* 1 eV *for*

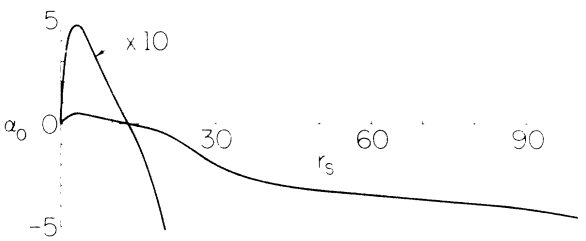

FIG. 9. Calculated exponent α_0 vs r_s: linear-response screening.

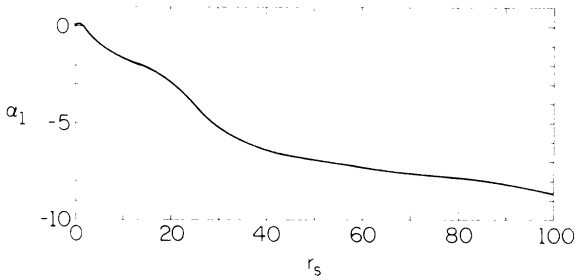

FIG. 10. Exponent α_1 vs r_s: linear-response screening.

Mg_xSb_{1-x} *or the Mahan threshold law is inapplicable to the* Mg_xSb_{1-x} $L_{2,3}$ *absorption edges.* If the Mahan theory does indeed describe the Mg_xSb_{1-x} data, then this conclusion supports a tentative identification $\xi = R$.[62]

V. CONCLUSIONS

The principal conclusions to be drawn from this work are the following: (i) The final-state interactions asymmetrically broaden the x-ray thresholds, as evidenced by the single-valued nature of the exponents α_0 as a function of r_s (for Na, Mg, and Al) and as a function of resistivity for amorphous Mg_xSb_{1-x} alloys. (ii) The Mahan form of the threshold anomaly Eq. (5) is supported by the analyses here; but, since there are so many adjustable parameters involved in fitting the spectra, it cannot be unequivocally stated that these analyses confirm and demonstrate the experimental validity of Mahan's threshold law. (iii) In Mahan's law, the most reasonable choice of the cutoff ξ is the exciton rydberg R, since $\xi \approx 0.24$ eV is independent of x for Mg_xSb_{1-x} data, but a more complicated dependence for ξ is quite possible. (iv) The expression [Eq. (8)] for the Mahan exponents α_l in terms of Fermi-energy phase shifts is inapplicable to the data analyzed here. The Li exponent α_0 derived using compatibility relationships from the K-edge exponent α_1 is inconsistent with the empirical rule $\alpha_0 = 0.068 r_s$, and the dependence of metallic L-edge exponents on r_s differs from that predicted using a screened electron-hole interaction. (v) So that the

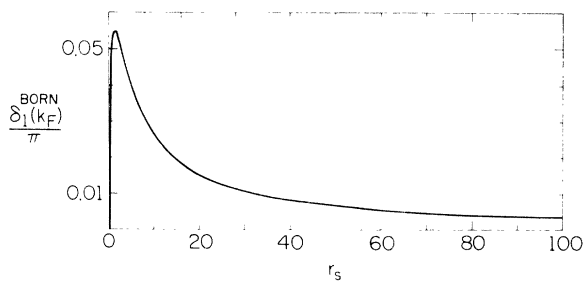

FIG. 11. Fermi-energy Born-approximation p-wave phase shift $\delta_1(k_F)$ plotted as δ_1/π vs r_s, as computed using linear-response screening.

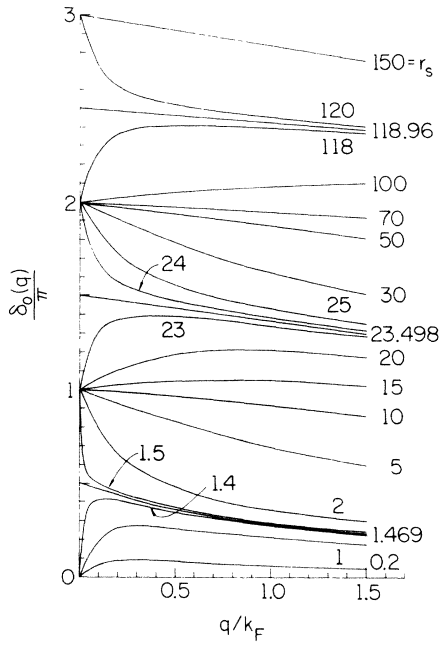

FIG. 12. Linear-response-screening approximation s-wave phase shift $\delta_0(q)$ plotted as δ_0/π vs momentum transfer q in units of Fermi momentum k_F. The various curves are labeled by the appropriate value of r_s. Note that the slope of δ_0 at $q=k_F$ is negative in the majority of cases, which corresponds to a negative time-delay.

exponents $\alpha_0(r_s)$ for alloys such as Mg_xSb_{1-x} can be compared directly with the theory, it would be useful to combine determinations of the mobility (i.e., r_s) as a function of composition x with analyses of the x-ray spectra.

ACKNOWLEDGMENTS

We gratefully acknowledge stimulating conversations with C. P. Flynn, D. L. Smith, and F. C. Brown.

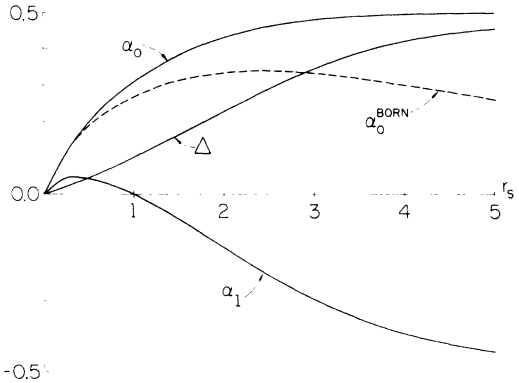

FIG. 13. Exponents α_0, α_1, Δ (Eq. (8)) vs r_s: self-consistent screening. The dashed line is the value of α_0 computed in the Born approximation.

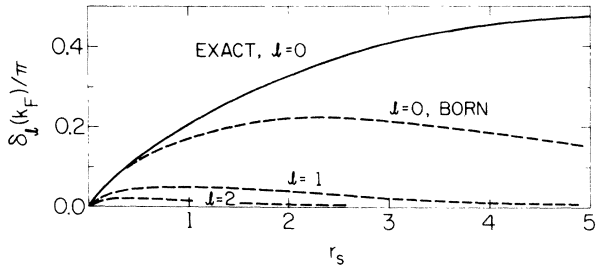

FIG. 14. Fermi-energy phase shifts $\delta_l(k_F)$ vs r_s: self-consistent screening. Solid line: $l=0$ exact phase shift; dashed lines: Born approximation.

APPENDIX A: THEORETICAL RESULTS, $r_s \geq 5$; LINEAR-RESPONSE SCREENING

We present here some results of our computations which may prove useful in future work. The calculations are based on Hulthén's potential and *linear-response* theory, as discussed in Sec. III A 1. The screening wave vector is

$$k_s^L a = 1.473 r_s^{-1/2}. \quad \text{(A. 1)}$$

The s-wave exponent α_0 [see Eq. (8)], calculated using the exact Hulthén s-wave phase shift and Born-approximation values of the other phase shifts, is plotted in Fig. 9 as a function of r_s. A similar graph of α_1 is given in Fig. 10. Both exponents have been evaluated assuming that Eq. (8) is valid for all values of phase shifts[42,63] and is not π periodic. It is quite possible that at least part of the exponent is π periodic.[42,64]

The Fermi-energy Born-approximation p-wave phase shift is plotted in Fig. 11. Unlike the exact phase shift, the Born value does not reflect bound p states for $r_s \gtrsim 30$, in which regime the correct value for the screened potential can be estimated

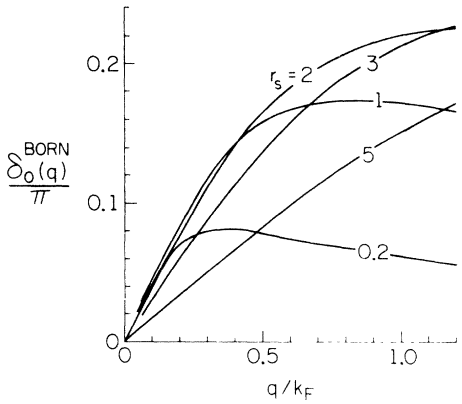

FIG. 15. Born-approximation s-wave phase shift vs momentum transfer q in units of Fermi momentum k_F: self-consistent screening. The values of r_s label the curves.

TABLE III. Spin-orbit energies W.

Metal	W (eV)
Na	0.16
Mg	0.27
Al	0.43

from Levinson's theorem[37] (since $E_F \to 0$ for $r_s \gg 1$):

$$\delta_1(k_F) \approx \delta_1(0) = n_p\pi. \quad \text{(A. 2)}$$

Here n_p is the number of bound p states in the screened potential for a particular value of r_s.

The s-wave phase shift as a function of momentum transfer q is plotted in Fig. 12 for various values of r_s. Observe that for $q \to 0$ the phase-shift reduces to $n_s\pi$, n_s is the number of bound s states; exceptions occur when a bound state has zero binding energy and the phase shift equals an integral multiple of $\frac{1}{2}\pi$.

APPENDIX B: THEORETICAL RESULTS, $r_s < 5$; SELF-CONSISTENT SCREENING

For $r_s < 5$, the screening wave vector was computed self-consistently according to the prescriptions set forth in Sec. III A 2 (see Fig. 4). Again the potential is

$$V_{eh} = \frac{-e^2 k_s \pi^2/6\epsilon_0}{e^{k_s \pi^2 r/6} - 1}. \quad \text{(B. 1)}$$

The exact value of the s-wave phase shift was computed, while higher angular momentum waves were treated in Born approximation. The exponents α_0, α_1, and Δ [see Eq. (8)] are graphed as a function of r_s in Fig. 13, along with α_0^{Born}, the value of α_0 obtained when the s-wave is treated in Born approximation.

The Fermi-energy phase shifts are given in Fig. 14. Born-approximation values of s and p phase shifts are given in Figs. 15 and 16.

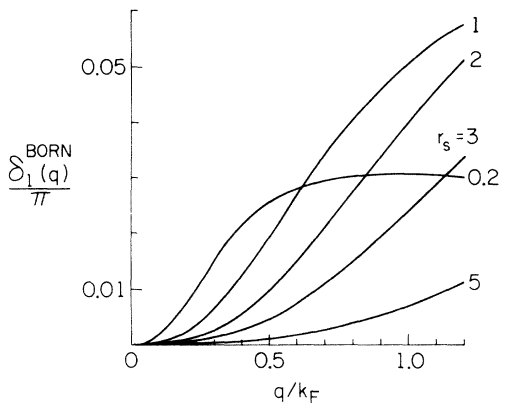

FIG. 16. Born-approximation p-wave phase shift vs momentum transfer q: self-consistent screening. The values of r_s label the curves.

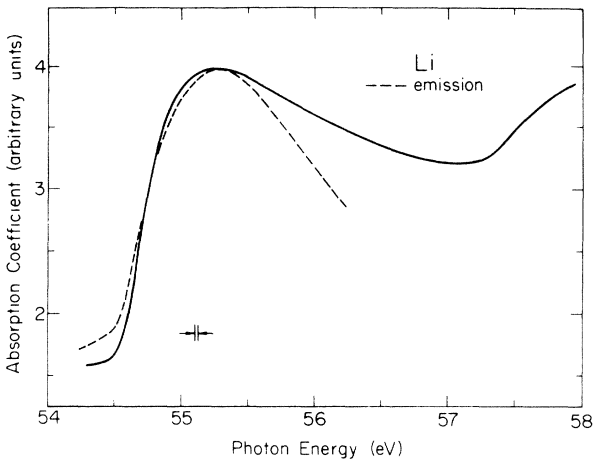

FIG. 17. Soft x-ray absorption spectrum of Li: absorption in arbitrary units vs photon energy $\hbar\omega$. After Ref. 4. The dashed line represents emission data, reflected in E_T, of O. Aita and J. Sagawa [J. Phys. Soc. Japan 27, 164 (1969)]. The experimental resolutions for the absorption data are indicated in Figs. 17–20.

APPENDIX C: SPECTRA OF Li, Na, Mg, and Al

The soft-x-ray absorption spectra of Li, Na, Mg, and Al are given in Figs. 17–20. The L_3 absorp-

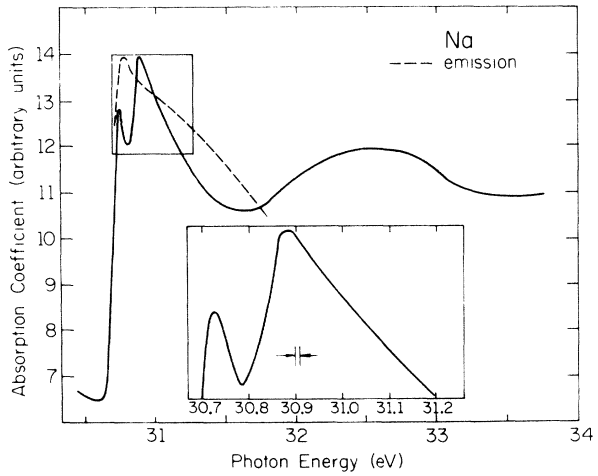

FIG. 18. Soft-x-ray absorption spectrum of Na, Ref. 4. The dashed line represents emissions data of R. S. Crisp and S. E. Williams [Phil. Mag. 6, 365 (1961)].

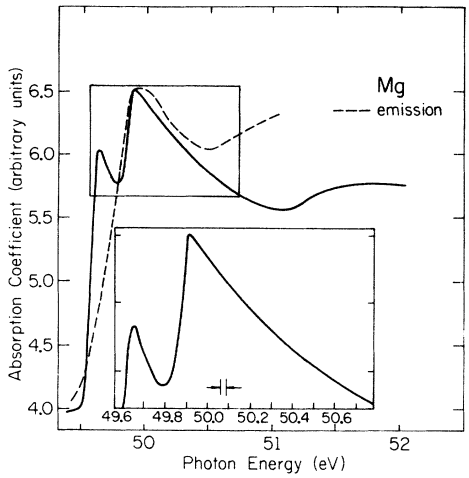

FIG. 19. Soft-x-ray absorption spectrum of Mg, Ref. 4. The dashed line represents emission data of L. M. Watson, R. K. Dimond, and D. J. Fabian, in *Soft X-ray Band Spectra*, D. J. Fabian, editor, (Academic, New York, 1968).

tion spectra were obtained from the original spectra by subtracting the L_2 component assuming that it has an identical shape $S(\omega)$ to that of the L_3 component, but shifted by the spin-orbit energies W listed in Table III:

$$\epsilon_2(\omega) = S(\omega) + CS(\omega - W) + B. \qquad \text{(C. 1)}$$

Absorption due to outer electrons was accounted for by a constant background B. Starting with the experimentally determined energy splitting between the L_2 and L_3 edges for W and the theoretical value $C = 0.5$, both the spin-orbit energy W and C were varied slightly. C and W were determined by the requirement that the subtracted spectra be smooth and free of structure periodic with the spin-orbit

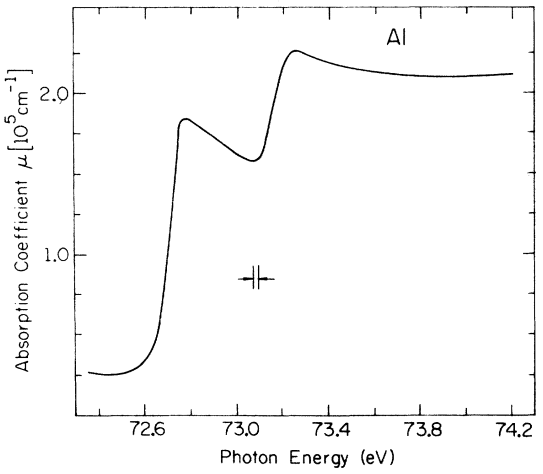

FIG. 20. Soft-x-ray absorption spectrum of Al, Ref. 4.

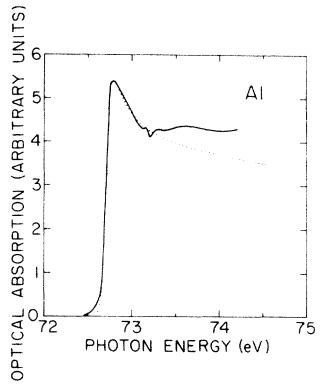

FIG. 21. Subtracted L_3 absorption spectrum of Al. The structure near 73.2 eV is associated with the subtraction process and should be smoothed. Solid line: data; dotted line: theory.

energy W. In fact, the L_2 and L_3 edges manifested somewhat different shapes, especially near threshold; such differences led to small oscillations in the subtracted spectra which subsequently were smoothed (see Fig. 21).

The smoothed subtracted spectra $\epsilon_2(\omega)$ were then fit with the formula

$$\epsilon_2(\omega) = \int_{E_T/\hbar}^{\infty} B(\hbar\omega - x) A^2 \xi^{\alpha} (x - E_T)^{-\alpha}\, dx, \qquad \text{(C. 2)}$$

where $B(x)$ is a Gaussian of width Γ. The constant $A^2\xi^{\alpha}$ was determined by requiring that the theoretical and experimental spectra coincide at some energy as far above threshold as reasonable (i.e.,

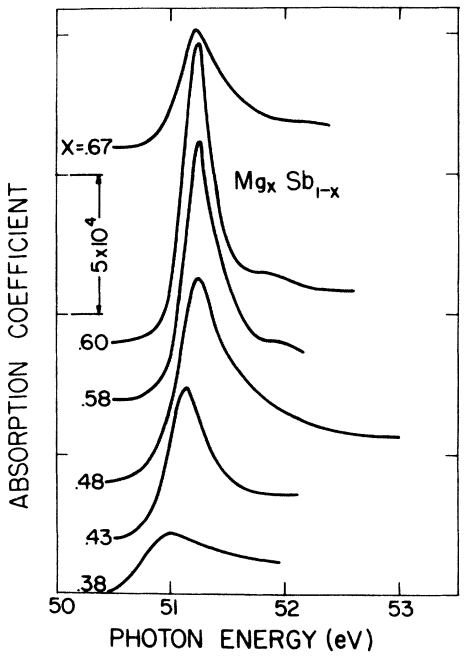

FIG. 22. Component absorption spectra for amorphous Mg_xSb_{1-x}. These spectra represent one component of the threshold doublet. Each curve is labeled according to composition x. All samples were deposited and measured below 100 K.

$\approx W$ above threshold) and E_T was estimated.[65] The parameters α and Γ were adjusted to provide an optimum fit.[66]

We were astounded to find both that the shape of the low-energy edge was compatible with only a small range of values for Γ and that the height and shape of the peak determined the exponent α with considerable precision. Illustrations of the fitting procedure have been published elsewhere.[67]

APPENDIX D: SPECTRA OF Mg_xSb_{1-x}

The subtracted spectra for amorphous alloys Mg_xSb_{1-x} are given in Fig. 22. The method by which exponents α were extracted is discussed by Slowik[6] and differs from the methods applied to Na, Mg, and Al in only one essential way: The subtracted spectra were not compared directly with the broadened Mahan law [Eq. (5)]. Instead the spectra were graphed logarithmically, $\ln\epsilon_2$ vs $\ln(\hbar\omega - E_T)$, and an exponent α estimated from the slope of the plotted curve. This procedure is discussed in Ref. 6 and is only slightly less satisfactory than fitting the broadened Mahan law [Eq. (5)] directly. Exponents extracted using this procedure tend to be too large by the negligible amount $\lesssim 0.04$ or ≈ 0.04.

---

*Research supported by the National Science Foundation under Grant Nos. NSF-GH-33634 and NSF-GH-39132.
†Research performed under the auspices of the U. S. Atomic Energy Commission.
‡Research supported in part by U. S. Army Research Office under Contract No. ARO-D-31-124-71-G15, by Advanced Research Projects Agency under Contract No. HC15-67-C-0021, and by the National Science Foundation under Grant No. NSF-GH-33634.
§Present address.
||Research supported in part by Xerox Corporation, Webster Research Center.
**Research supported in part by the National Science Foundation under Grant No. NSF-GH-33634 and the U. S. Army Research Office (Durham) under Contract No. DA-ARO-D31-124-71G103.

[1]G. D. Mahan, Phys. Rev. 163, 612 (1967).
[2]For a review of the theory and the data, see G. D. Mahan, in *Solid State Physics*, edited by F. Seitz, D. Turnbull, and H. Ehrenreich (Academic, New York, 1973), Vol. 29.
[3]See, e.g., J. J. Hopfield, Comments Solid State Phys. II, 40 (1969); V. J. Emery and A. Luther, Phys. Rev. B 9, 215 (1974).
[4]C. Kunz, R. Haensel, G. Keitel, P. Schreiber, and B. Sonntag, in *Electronic Density of States*, edited by L. H. Bennett, Natl. Bur. Stds. Spec. Publ. No. 323 (U. S. GPO, Washington, D. C.), p. 275.
[5]J. H. Slowik and F. C. Brown, Phys. Rev. Lett. 29, 934 (1973). The exponents listed in this Letter are different from the improved values listed in Table I of the present work and in Ref. 6.
[6]J. H. Slowik, preceding paper, Phys. Rev. B 10, 416 (1974). An exponent $\alpha_0 > 1$ extracted from an unbroadened spectrum would violate the oscillator-strength sum rule. However for a broadened spectrum, uncertainty in the fitting procedure permits $\alpha_0 > 1$.
[7]The hole mass is assumed infinite.
[8]For example, using the random-phase-approximation expression for the dielectric constant [see, e.g., P. Nozières and D. Pines, Nuovo Cimento 9, 470 (1958)], only those virtual excited states with a hole in some core level would be summed over.
[9]G. D. Mahan, J. Res. Natl. Bur. Stand. A 74, 267 (1970).
[10]G. Ausman, Jr. and A. J. Glick, Phys. Rev. 183, 687 (1969); Phys. Rev. B 1, 942 (1970); P. Longe, Phys. Rev. B 8, 2572 (1973).
[11]For simplicity, all calculations presented in this paper refer to the zero-temperature limit.
[12]P. Nozières and C. T. DeDominicis, Phys. Rev. 178, 1097 (1969).
[13]In terms of the absorption coefficient $K_A(\omega)$, $\epsilon_2(\omega) = (c\eta(\omega)/\omega)K_A(\omega)$, where c is the speed of light and η is the index of refraction.
[14]This explanation has been challenged. See Refs. 15–17.
[15]J. D. Dow, Phys. Rev. Lett. 31, 1132 (1973).
[16]J. D. Dow, L. N. Watson, and D. J. Fabian, J. Phys. F (to be published); J. D. Dow, Phys. Rev. B (to be published).
[17]J. D. Dow, J. E. Robinson, and T. R. Carver, Phys. Rev. Lett. 31, 759 (1973).
[18]P. W. Anderson, Phys. Rev. Lett. 18, 1049 (1967); Phys. Rev. 164, 352 (1968).
[19]E. Burstein, Phys. Rev. 93, 632 (1954); M. Tanenbaum and H. B. Briggs, *ibid.* 91, 1561 (1953).
[20]G. Busch, F. Hulliger, and U. Winkler, Helv. Phys. Acta 27, 249 (1954).
[21]V. P. Zhuze, I. V. Mochan, and S. M. Ryvkin, Zh. Tekh. Fiz. 18, 1494 (1948).
[22]$\epsilon_0 \approx 1 + (\hbar\omega_p/\bar{E}_g)^2$, where $\hbar\omega_p$ is the plasmon energy and $\bar{E}_g$ is the average energy gap. $\epsilon_0 \approx 13$ is typical of a small-gap semiconductor.
[23]This model of the Mg_xSb_{1-x} alloys is a somewhat simplified version of one first suggested by Ferrier and Herrell in Ref. 24. The conclusions of this paper depend on the applicability of the model and Mahan's Hamiltonian to the alloys is question.
[24]R. P. Ferrier and D. J. Herrell, J. Non-Cryst. Solids 2, 278 (1970).
[25]K. Läuger (unpublished). See G. Wiech, in *Soft X-ray Band Spectra*, edited by D. J. Fabian (Academic Press, London, 1968), p. 62.
[26]H. Neddermeyer, in *Band Structure Spectroscopy of Metals and Alloys*, edited by D. J. Fabian and L. M. Watson (Academic, London, 1973), p. 153.
[27]H. Neddermeyer, Phys. Lett. A 44, 181 (1973).
[28]H. W. Wolff, K. Radler, B. Sonntag, and R. Haensel, Z. Phys. 257, 353 (1972).
[29]B. F. Sonntag, J. Phys. F 3, L255 (1974).
[30]J. D. Dow and D. L. Smith, J. Phys. F 3, L170 (1973).
[31]J. D. Dow, J. E. Robinson, and T. R. Carver, Phys. Rev. Lett. 31, 759 (1973); D. R. Franceschetti and J. D. Dow, J. Phys. F (to be published).
[32]J. D. Dow, Phys. Rev. Lett. 31, 1132 (1973). Although the K-edge data have been doubly revised (see Refs. 26 and 27), the conclusions of this paper remain valid. See also N. H. March, Ref. 26, p. 297.

[33]J. D. Dow (unpublished); P. Longe, Phys. Rev. B 8, 2572 (1973).

[34]J. D. Dow, Phys. Rev. B (to be published).

[35]See, e.g., C. Kittel, *Quantum Theory of Solids* (Wiley, New York, 1963), p. 106.

[36]See, e.g., A. G. Sitenko, *Lectures in Scattering Theory* (Pergamon, New York, 1971).

[37]See, e.g., N. F. Mott and H. S. W. Massey, *The Theory of Atomic Collisions*, 3rd ed. (Clarendon, Oxford, England, 1965), p. 156. We follow the convention $\delta_l(\infty)=0$.

[38]Even in this regime, we shall assume zero temperature.

[39]We have used the integral $\int_0^\infty x^{\nu-1}dx/(e^{\mu x}-1)=\mu^{-\nu}\Gamma(\nu)\zeta(\nu)$ for $\mathrm{Re}\mu>1$, and the identity $\sum_{l=0}^{\infty}(2l+1)j_l^2(x)=1$. See, e.g., I. S. Gradshteyn and I. W. Ryzhik, *Tables of Integrals Series and Products*, 4th ed., (Academic, New York, 1965), p. 235; and M. Abramowitz and I. A. Stegun, *Handbook of Mathematical Functions*, Natl. Bur. Stds. AMS 55 (U. S. GPO, Washington, D. C., 1964), pp. 253, 811, and 440. See also F. Stern, Phys. Rev. 158, 697 (1967).

[40]If the actual s-wave phase-shift exceeds the Born-approximation value by $\frac{1}{2}Z\pi$, there is no solution, since all the Born-approximation phase shifts are positive.

[41]F. Brouers, P. Longe, and B. Bergersen, Solid State Commun. 8, 1423 (1970); P. Longe, Phys. Rev. B 8, 2572 (1973).

[42]J. Friedel, Comments Solid State Phys. 2, 21 (1969).

[43]W. J. Pardee and G. D. Mahan, Phys. Lett. A 45, 117 (1973). The threshold formula given by these authors has been evaluated and shown to be insignificantly different from the MND result [J. D. Dow, J. E. Robinson, and T. R. Carver (unpublished)].

[44]K. M. Watson, Phys. Rev. 95, 228 (1954).

[45]R. J. Elliott, Phys. Rev. 108, 1384 (1957).

[46]See, e.g., R. A. Ferrell, Phys. Rev. 186, 399 (1969).

[47]It has been stated that ξ should be taken to be a typical conduction bandwidth, but this is not generally the case, as may be seen by considering the limit of zero free charge in the conduction band ($r_s\to\infty$). Mahan formulated his model with the intention of reproducing the Elliott exciton theory in this limit, giving an absorption proportional both to the square of the electron's overlap with the massive hole localized at the origin and to the density of final states $\epsilon_2(\omega)\propto\sum_\nu|\psi_\nu(0)|^2\times\delta(\hbar\omega-E_{\mathrm{gap}}-E_\nu)$. The envelope function ψ_ν satisfies the exciton effective-mass Schrödinger equation, which (in the limit of infinite hole-mass) is $[(-\hbar^2/2m)\nabla^2+V_{\mathrm{eh}}]\psi_\nu(\vec{\mathbf{r}})=E_\nu\psi_\nu(\vec{\mathbf{r}})$, where, in the Wannier-exciton limit, the electron-hole interaction *should be* $V_{\mathrm{eh}}=-e^2/\epsilon_0 r$. In order to have a tractable model of the degenerate Fermi-gas limit ($r_s\lesssim 10$), Mahan was forced to replace V_{eh} with a δ-function contact interaction $V_{\mathrm{eh}}=-\lambda\delta(\vec{\mathbf{r}})$, where λ is a positive constant with dimensions of energy times volume. But the δ function scatters the electron with all possible momentum transfers equally well, leading to divergent and unphysical results. Therefore it is necessary to introduce a cutoff energy ξ to avoid the spurious divergence. (A similar cutoff is necessary for the separable potential of Nozières and DeDominicis.) This is easily accomplished by taking the density of conduction-band states $N_c(E)$ to be a square-root function of energy, cut off at ξ (Fig. 5) $N_c(E)=(2m/\hbar^2)^{3/2}\times(4\pi^2)^{-1}E^{1/2}\theta(E)\theta(\xi-E)$. Here the zero of energy is at the bottom of the conduction band. In this formulation, ξ has the *appearance* of being the conduction-band width. But recall that, in the effective-mass limit of zero free-charge density, there is *no need to introduce* ξ *if the Coulombic form of the electron-hole interaction is used*; hence, ξ is a mathematical parameter without physical relevance.

[48]Here we consider only one term of Eq. (5), taking the value of l for which α_l is largest and Eq. (5) most divergent (normally α_0). Near threshold, this approximation introduces negligible error. By making this approximation, we avoid specifying the unknown ξ, since $A\xi^{\alpha}$ is a single fitting parameter, rather than A_l and ξ separately. For example, a crude estimate of the relative sizes of the $l=2$ and 0 contributions to Eq. (5) for $L_{2,3}$ edges is $(A_2/A_0)^2(\Gamma/\xi)^{\alpha_0-\alpha_2}\approx 0.1(A_2/A_0)^2$. Careful analysis [J. D. Dow, D. L. Smith, and B. F. Sonntag, Phys. Rev. B (to be published)] of the d-wave contribution as a function of A_l, α_l, Γ, and ξ reveal that, even under pessimistic conditions, the exponent α extracted using only one term of Eq. (5) is smaller than the actual exponent α_0 by only ≈ 0.08. If such a correction is indeed called for, the extract $L_{2,3}$ exponent of potassium (with $r_s=4.86$) should differ from the empirical rule, Eq. (33). A more optimistic estimate of the d-wave corrections is that they are a negligible 10%.

[49]That is, convolved with the broadening function $B(x)=(2\pi^2\Gamma)^{-1/2}\exp[-\frac{1}{2}(x/\Gamma)^2]$.

[50]J. T. Yue and S. Doniach, Bull. Am. Phys. Soc. 18, 456 (1973); Phys. Rev. B 8, 4578 (1973).

[51]In fitting spiked absorption edges, the breadth of the low-energy edge sensitively determines the broadening Γ; then the size of the peak and its high-energy slope precisely define α.

[52]See Fig. 3 of Ref. 24.

[53]While the possibility that holes contribute to the conduction cannot be ruled out experimentally, we note that application of the Mahan theory to Mg_xSb_{1-x} presumes the simple band-structure model of a degenerate parabolic conduction band and a narrow core band; in this model, only electrons conduct.

[54]It is likely that the mobility for Mg_xSb_{1-x} may exhibit a "mobility edge" as the conduction changes from coherent flow to incoherent hopping. This argument applies only to the coherent case.

[55]A case in point is provided by the drift mobility in degenerate n-type GaSb, where the density of states at the Fermi surface rapidly increases with density by a factor of 5 as the sidebands are populated, but the drift mobility increases only by a factor of 2. See e.g., J. E. Robinson and S. Rodriguez, Phys. Rev. 137, A663 (1965).

[56]Note that the datum for $x=0.67$, which corresponds to the thinnest Mg_xSb_{1-x} appears to be separate from the other data. However, the measurements of resistivity vs x (Ref. 24) and $\alpha_0(x)$ (Refs. 5,6) have a combined uncertainty in x of approximately 4%; furthermore the resistivity data were taken at 273 K whereas the x-ray absorption experiment was performed at 100 K. The relatively small uncertainty in x is amplified by the resistivity, which abruptly changes by nine orders of magnitude on the Mg-rich side of the intermetallic composition $x=0.6$. Thus some of the data for $\alpha_0(\rho)$ have enormous resistivity error bars attributable to the sharp resistivity shoulder.

[57]It is, of course, possible that Mg_xSb_{1-x} alloys have a complicated band structure with, for example, heavy-

mass indirect conduction bands. In such a case, it would be possible for r_s to vary while E_F remained virtually constant.

[58]W. E. Spear, J. Non-Cryst. Solids 1, 197 (1969).

[59]J. D. Dow and B. F. Sonntag, Phys. Rev. Lett. 31, 1461 (1973).

[60]$\epsilon_2(\Omega)$ is not measured directly. Rather, the form Eq. (27) for $\epsilon_2(\omega)$ is fit to the edge shape for $\hbar\omega \approx E_T$ and $\epsilon_2(\Omega)$ determined from the extrapolated fit, since the form Eq. (27) may not be valid 1 eV above threshold. A is proportional to a transition matrix element, whose size is determined mainly by quasiatomic properties. Thus, to a fair approximation, A^2/x should be independent of composition x, especially since most of the data correspond to compositions near $x = 0.6$, the intermetallic compound.

[61]The data are insufficiently precise to rule out curvature; but they do exclude the possibility $\xi > 1$ eV.

[62]The exciton rydberg and the dielectric constant ϵ_0 are not precisely known and are likely to be functions of composition. However, ϵ_0 is likely to be large, since Mg_3Sb_2 is a semiconductor, and most of the data correspond to compositions near $x = 0.6$. Thus the estimate of Sec. II, $R \approx 0.25$ eV, should be semiquantitatively reliable.

[63]M. Combescot and P. Nozières, J. Phys. (Paris) 32, 913 (1971).

[64]N. Rivier and E. Simanek, Phys. Rev. Lett. 26, 435 (1971); C. P. Flynn, Phys. Rev. Lett. 32, 1059 (1974).

[65]The threshold energy was taken to be at the center of the abrupt absorption edge.

[66]$\Gamma = 0.05 \pm 0.04$ for all spectra. The results are insensitive to choices of Γ within this range.

[67]J. D. Dow, D. L. Smith, and B. F. Sonntag, Phys. Rev. B (to be published).